

# Solution-Processable Multifused Thiophene Small Molecules and Conjugated Polymer Semiconducting Blend for Organic Field Effect Transistor Application

Shakil N. Afraj, Guan-Yu He, Chih-Yu Lin, Arulmozhi Velusamy, Chu-Yun Huang, Po-Shen Lin, Sureshrajju Vegiraju, Ping-Yu Huang, Jen-Shyang Ni, Shueh-Lin Yau, Shih-Huang Tung, Takeo Minari, Cheng-Liang Liu,\* and Ming-Chou Chen\*

Three new solution-processable organic semiconductors (1–3) are synthesized and characterized for p-type organic field effect transistors (OFETs). The backbone of these small molecules is modified by expanding the central core conjugation from thienothiophene (TT) to dithienothiophene (DTT) and tetrathienoacene (TTA), which are end-capped with soluble  $\beta$ -substituted alkyl chains dithienothiophenes (DTTR) to generate DTTR-TT (1), DTTR-DTT (2), and DTTR-TTA (3). The highest mobility of  $0.016 \text{ cm}^2 \text{ V}^{-1} \text{ s}^{-1}$  is achieved using solution-sheared DTTR-TTA film due to the extended conjugated TTA core, which enhances the intermolecular interaction and generates an efficient percolation for the OFET channel. Solution blending of crystalline DTTR-TT small molecules with oriented-packing polymer dithienothiophene-thioalkylbithiophene (PDTT-SBT) polymer leads to significantly enhanced mobilities from  $0.0009$  up to  $0.22 \text{ cm}^2 \text{ V}^{-1} \text{ s}^{-1}$ , occurring at an optimized 30% DTTR-TT composition in the blend. Hole mobility of 30% DTTR-TT blend is  $0.22 \text{ cm}^2 \text{ V}^{-1} \text{ s}^{-1}$  which is higher than pristine small molecule DTTR-TT ( $0.0009 \text{ cm}^2 \text{ V}^{-1} \text{ s}^{-1}$ ) and polymer PDTT-SBT ( $0.067 \text{ cm}^2 \text{ V}^{-1} \text{ s}^{-1}$ ), respectively. An efficient strategy to enhance the mobility of small molecule DTTR-TT by blending with easily synthesizable PDTT-SBT polymer is reported.

## 1. Introduction

Organic semiconductors are of potential interest due to their high throughput, inexpensive production, mechanical flexibility, light weight, and efficient integration within the supply chain, as well as great potential for new foundational studies.<sup>[1–13]</sup> Over the past 20 years, a number of small molecules have been successfully used in organic thin film transistors (OFETs).<sup>[14–18]</sup> Along with their significant structural versatility, facile synthesis, high purity, better reproducibility, and reliability without batch-to-batch variations, small molecules possess controllable electronic and physical properties as compared to polymers.<sup>[19,20]</sup> Therefore, the development of novel small molecular organic materials for OFETs has become increasingly important. The design of small molecular organic semiconductors should include a highly planar conjugated core for efficient charge transport,

Dr. S. N. Afraj, A. Velusamy, C.-Y. Huang, Dr. S. Vegiraju, P.-Y. Huang, Prof. S.-L. Yau, Prof. M.-C. Chen  
Department of Chemistry and Research Center of New Generation Light Driven Photovoltaic Modules  
National Central University  
Taoyuan 32001, Taiwan  
E-mail: mcchen@ncu.edu.tw


G.-Y. He, C.-Y. Lin  
Department of Chemical and Materials Engineering  
National Central University  
Taoyuan 32001, Taiwan

P.-S. Lin, Prof. C.-L. Liu  
Department of Materials Science and Engineering  
National Taiwan University  
Taipei 10617, Taiwan  
E-mail: liucl@ntu.edu.tw

Prof. J.-S. Ni  
Department of Chemical and Materials Engineering  
Photo-Sensitive Material Advanced Research and Technology Center (Photo-SMART)  
National Kaohsiung University of Science and Technology  
Kaohsiung 80778, Taiwan

Prof. S.-H. Tung  
Institute of Polymer Science and Engineering  
National Taiwan University  
Taipei 10617, Taiwan

Prof. T. Minari  
Research Center for Functional Materials  
National Institute for Materials Science  
1-1 Namiki, Tsukuba, Ibaraki 305-0044, Japan

 The ORCID identification number(s) for the author(s) of this article can be found under <https://doi.org/10.1002/admt.202001028>.

DOI: 10.1002/admt.202001028

favorable intermolecular  $\pi$ - $\pi$  stacking, and the presence of alkyl chains, which increases solubility and enables solution processability. Among the various conjugated building blocks that have been developed, fused thiophenes, such as thienothiophene (TT), dithienothiophene (DTT), and tetrathienoacene (TTA), have received extensive attention due to their structural planarity and strong intermolecular S...S interactions, which promote intramolecular and intermolecular  $\pi$ - $\pi$  stacking,<sup>[21–28]</sup> and thus superior carrier transfer efficiency.<sup>[29,30]</sup> Therefore, utilization of these units in the design of new solution processable organic semiconductors for OFET applications is highly desirable. Several solution-processable fused thiophene-based organic semiconductors have been developed.<sup>[27,29,31–33]</sup> For example, difluorene-thienothiophene (DDFTT)<sup>[34]</sup> and dithienothiophene-diketopyrrolopyrrole (DTT2DPP)<sup>[35]</sup> (Figure S1a, Supporting Information) exhibit mobilities of 0.0225 and 0.017 cm<sup>2</sup> V<sup>-1</sup> s<sup>-1</sup>, respectively. Furthermore, more conjugated tetrathienocene-based small molecules diketopyrrolopyrrole-tetrathienoacene (DDPP-TTAR)<sup>[25]</sup> and thiophenylvinylthiophene-tetrathienoacene (DTVT-TTAR)<sup>[36]</sup> (Figure S1a, Supporting Information) exhibit higher mobilities of 0.1 and 0.18 cm<sup>2</sup> V<sup>-1</sup> s<sup>-1</sup>, respectively. In addition, fused thiophenes are excellent spacers for organic dyes. For example, TTAR-based dyes exhibit power conversion efficiencies of up to 10.1% in dye-sensitized solar cells.<sup>[23,37]</sup>

Blending materials to combine the beneficial properties of multiple compounds within a single phase is commonly used in the field of organic electronics.<sup>[38–42]</sup> Small molecule semiconductors are well-known to exhibit excellent electrical properties as a result of high level of crystallinity and close  $\pi$ -overlap between molecules. However, they are difficult to process from the solution phase and tend to suffer from aggregation, forming microscopic crystals without interfacing with the metal contact.<sup>[43–45]</sup> Conversely, semicrystalline conjugated polymer-based assemblies have advantages with regard to solution-processing and morphology control, but relatively limited electrical properties due to the disorder in the materials.<sup>[39,46]</sup> The combined features of each material type with regard to the inherent superior crystallinity of small molecules and solution-processing/film-formation qualities of polymer binder, produce a prominent semiconducting blend system where the molecular component is either p-type or n-type. When using these blends for OFETs, the measured mobilities are expected to exhibit improved charge transport characteristics through the increased molecular organization if the connectivity solution-processed film with a charge carrier percolation pathway is predominantly generated.<sup>[47–53]</sup> More interestingly, the relationship between the morphology and charge transport in the conjugated small molecule/polymer semiconducting blend system can be established. Moreover, among the large number of new material systems developed over the past decade, binary semiconducting blends, consisting of a small molecule and a conjugated polymer, have proven highly successful primarily due to their good performance.<sup>[39,50,54]</sup>

In particular, 5,5'-bis(4-n-hexylphenyl)-2,2'-bithiophene (dH-PTTP),<sup>[45]</sup> 2,8-difluoro-5,11-bis(triethylsilylethynyl) anthrathiophene (DiF-TESADT),<sup>[55]</sup> and 2,7-dioctyl[1]benzothieno[3,2-b][1]benzothiophene (C8-BTBT)<sup>[56]</sup> (the structures shown in Figure 1) blended with conjugated polymers have been widely investigated.<sup>[42]</sup> For instance, pure dH-PTTP exhibits

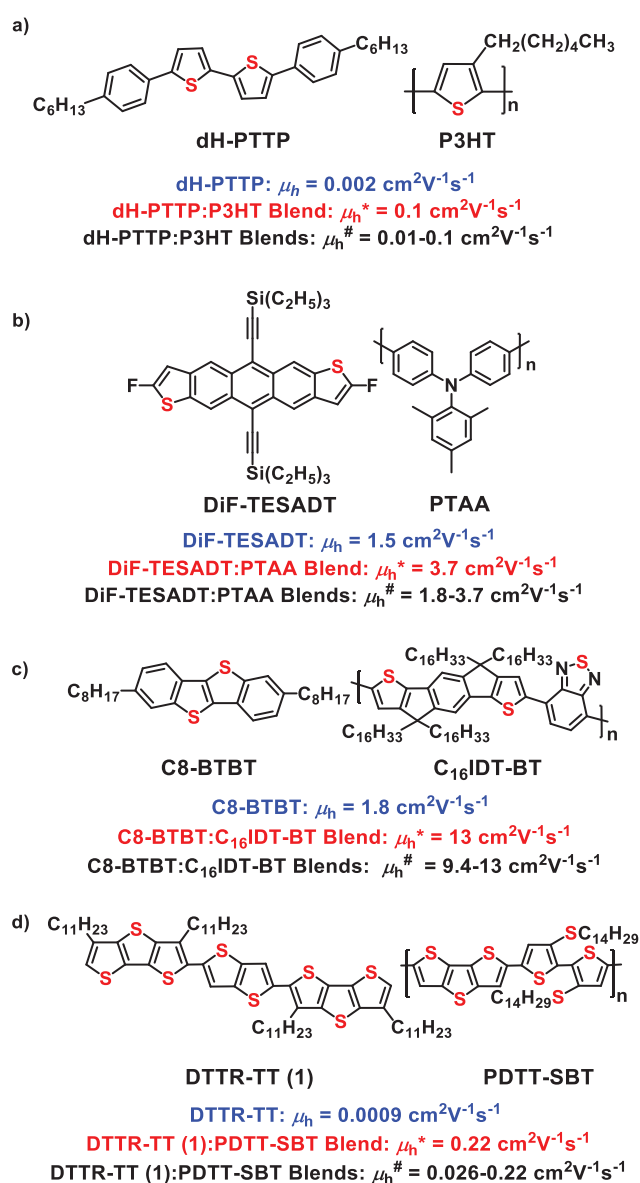


**Figure 1.** Chemical structures of small molecules and conjugated polymers: a) dH-PTTP and P3HT, b) DiF-TESADT and PTAA, c) C8-BTBT and C<sub>16</sub>IDT-BT, and d) DTTR-TT (1) semiconductor and conjugated polymer PDTT-SBT examined in this study.  $\mu_h$  denotes the hole mobility of the pure semiconductor,  $\mu_h^*$  denotes the highest mobility for the small molecule-conjugated polymer blend.  $\mu_h^\#$  denotes the mobility in range for the semiconductor-conjugated polymer blends.

a mobility of 0.002 cm<sup>2</sup> V<sup>-1</sup> s<sup>-1</sup>,<sup>[45]</sup> which could be enhanced to 0.1 cm<sup>2</sup> V<sup>-1</sup> s<sup>-1</sup> by blending it with poly(3-hexylthiophene-2,5-diyl) (P3HT) polymer (Figure 1a). Similarly, DiF-TESADT and C8-BTBT small molecules when blended with conjugated polymers such as poly[bis(4-phenyl)(2,4,6-trimethylphenyl)amine] (PTAA) and indacenodithiophene-benzothiadiazole (C<sub>16</sub>IDT-BT) their mobilities could be increased from 1.5<sup>[55]</sup> and 1.8 cm<sup>2</sup> V<sup>-1</sup> s<sup>-1</sup>,<sup>[56]</sup> for the pure systems, respectively, to 3.7<sup>[57]</sup> and 13 cm<sup>2</sup> V<sup>-1</sup> s<sup>-1</sup>,<sup>[58]</sup> respectively (Figure 1b,c). Note, different blend ratios can strongly affect OFET mobility which can vary 0.01–0.1 cm<sup>2</sup> V<sup>-1</sup> s<sup>-1</sup> for dH-PTTP-polymer blends,<sup>[45]</sup>

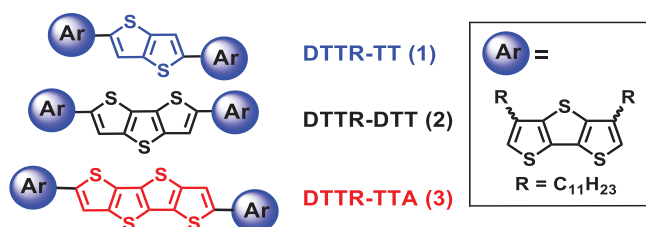


**Figure 2.** Chemical structures of the studied organic semiconductors 1–3.

1.8–3.7  $\text{cm}^2 \text{V}^{-1} \text{s}^{-1}$  for DiF-TESADT polymer blends,<sup>[57,59,60]</sup> and from 9.4 to 13  $\text{cm}^2 \text{V}^{-1} \text{s}^{-1}$  for the C8-BTBT-polymer blends.<sup>[49,58]</sup> Additionally, it has been shown that charge carrier mobilities are strongly dependent upon the blend composition,<sup>[45,57,58,61]</sup> therefore it would be desirable to investigate blend OFETs by using small molecule and conjugated polymer which could be easily synthesized from readily available starting materials.

In this work, considering the importance of fused thiophenes derivatives, we report three new small molecular organic semiconductors for p-type OFETs. TT, DTT, and TTA backbones were used as the central cores, which were coupled with soluble end-capped DTT with  $\beta$ -substituted alkyl side chains (DTTR) to afford DTTR-TT (1), DTTR-DTT (2), and DTTR-TTA (3), respectively (the structures shown in **Figure 2**). A comparative study of these organic semiconductor films reveals how the chemical structures, film crystallinity, and morphology affect the electrical properties of OFETs. Note that the maximum mobilities ( $\mu_{\text{max}}$ ) of 0.016, 0.0023, and 0.0009  $\text{cm}^2 \text{V}^{-1} \text{s}^{-1}$  were achieved from solution-sheared DTTR-TTA, DTTR-DTT, and DTTR-TT films, respectively. To further improve overall mobility, the low performed DTTR-TT molecule was incorporated with PDTT-SBT<sup>[62]</sup> polymer (structure shown in Figure 1d) upon modulating the composition ratio of two compounds in the blend, achieving the highest mobility of 0.22  $\text{cm}^2 \text{V}^{-1} \text{s}^{-1}$  measured in 30%:70% DTTR-TT:PDTT-SBT in weight ratio. It should be noted that the mobility value of DTTR-TT:PDTT-SBT blend is 250 and 3 times higher than that of pristine DTTR-TT (0.0009  $\text{cm}^2 \text{V}^{-1} \text{s}^{-1}$ ) and PDTT-SBT (0.067  $\text{cm}^2 \text{V}^{-1} \text{s}^{-1}$ ). To the best of our knowledge, these are the highest mobility values reported to date using the  $\beta$ -alkylated fused thiophenes as the end-capping units for solution-processable OFETs and its blends. DTTR-TT (1) and PDTT-SBT components used in the blending strategy are easily synthesizable by using an inexpensive starting material.<sup>[62]</sup>

In this paper, we choose DTTR-TT as dopant with the matrix of PDTT-SBT because we synthesize DTTR-TT from TT as central core, and TT unit is easy to synthesize from readily available starting material in good yield,<sup>[63,64]</sup> and further DTTR-TT (1) can be synthesized in more amount for device purposes. Herein, we find that the utilization of DTTR-TT small molecule in blending strategy is cost effective. Whereas DTT and TTA cores are hard to make and yields are low,<sup>[33,63]</sup> therefore getting more materials of DTTR-DTT and DTTR-TTA for larger scale device production is considerably very difficult. Moreover, DTTR-TT has a huge difference in mobility value as compared with pristine PDTT-SBT polymer, the improved performance is quite significant and we believe that the blend concept would be a general case and extended to the other two small molecules. Conceptually, for the small molecule to have a good backbone stacking with the polymer backbone, the alkyl chains on the  $\beta$ -position of fused

thiophene ( $\beta$ -DTTR-TT) should be better. As exhibited in Figure S1b (Supporting Information), during the stacking of  $\beta$ -DTTR-TT with polymer, the long alkyl chains at the  $\beta$ -position of end-capped unit will be more beneficial because of its efficient hole transfer property and good solubility. In detail, alkyl chains at the  $\beta$ -position of the DTTR unit enhance hole transfer efficiency via small molecule backbone to the polymer backbone. Moreover,  $\beta$ -DTTR-TT with four alkyl chains on one backbone unit greatly enhances the solubility of the compound and provides solution-processable OFET. Due to these significance advantages, in this paper we have designed  $\beta$ -alkylated DTTR end-capped unit based organic semiconductor and blends of small molecule and conjugated polymer have been explained.

## 2. Experimental Section

### 2.1. Materials

All chemicals and solvents were of reagent or anhydrous grade and were obtained from Aldrich, Alfa, and TCI Chemical Co. Solvents for reactions (toluene and tetrahydrofuran) were distilled under nitrogen from sodium/benzophenone ketyl, and halogenated solvents were distilled from  $\text{CaH}_2$ . Dialkyldithienothiophene (5), monobromodialkyldithienothiophene (6), 2,5-bis(tributylstannyl)thieno[3,2-*b*]thiophene, 2,6-bis(tributylstannyl)dithieno[3,2-*b*:2',3'-*d*]thiophene, and 2,6-bis(tributylstannyl)thieno[2',3':4,5]thieno[3,2-*b*]thieno[2,3-*d*]thiophene were prepared according to the procedures described in the literature.<sup>[63,65]</sup> PDTT-SBT (4) polymer was also synthesized according to a procedure described in the literature.<sup>[62]</sup>

### 2.2. General Synthetic Procedures for the Target Compounds (1–3)

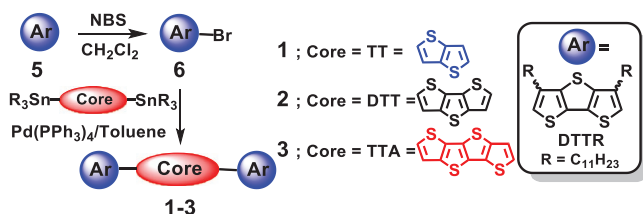
Under anhydrous condition,  $\text{Pd}(\text{PPh}_3)_4$  (0.05 equiv) was added to a solution of monobromodialkyldithienothiophene (6, 2.1 equiv.) and distannylated compound (1 equiv.) in dry toluene. The resulting mixture was refluxed for 48 h under nitrogen. After the reaction solvent was evaporated, the desired product was purified by column chromatography using ethyl acetate and hexanes. It was further purified by being recrystallized from toluene.

#### 2.2.1. DTTR-TT (1)

Compound 1 was obtained as an orange solid (yield = 68%). Mp: 121 °C.  $^1\text{H}$  NMR (300 MHz,  $\text{CDCl}_3$ )  $\delta$ : 7.29 (s, 2 H), 6.98 (s, 2 H), 2.95 (t,  $J = 7.5$  Hz, 4H), 2.74 (t,  $J = 7.5$  Hz, 4H), 1.79 (m, 8H), 1.35 (br, 64H), 0.88 (m, 12H);  $^{13}\text{C}$  NMR (75 MHz,  $\text{CDCl}_3$ )  $\delta$ : 143.06, 141.36, 139.44, 138.14, 136.19, 133.30, 130.82, 130.50, 129.12, 120.80, 117.92, 32.00, 29.75, 29.45, 29.26, 28.96, 28.74, 22.78, 14.20; HRMS ( $m/z$ , FAB+) calcd for  $\text{C}_{66}\text{H}_{96}\text{S}_8$ , 1144.5278; found: 1144.5272.

#### 2.2.2. DTTR-DTT (2)

Compound 2 was obtained as an orange crystalline solid (yield = 61%). Mp: 116 °C.  $^1\text{H}$  NMR (300 MHz,  $\text{CDCl}_3$ )  $\delta$ : 7.31 (s, 2H), 6.98 (s, 2 H), 2.95 (t,  $J = 7.5$  Hz, 4H), 2.74 (t,  $J = 7.5$  Hz,



**Scheme 1.** Synthetic route to organic semiconductors 1–3.

4 H), 1.79 (m, 8 H), 1.35 (br, 64 H), 0.88 (m, 12H).  $^{13}\text{C}$  NMR (75 MHz,  $\text{CDCl}_3$ )  $\delta$ : 143.07, 141.39, 141.30, 137.21, 136.17, 133.24, 130.65, 130.46, 129.04, 120.78, 119.03, 32.00, 29.74, 29.49, 29.44, 29.21, 28.96, 28.73, 22.77, 14.20; HRMS ( $m/z$ , FAB+) calcd for  $\text{C}_{68}\text{H}_{96}\text{S}_9$ , 1200.4998; found: 1200.4983.

### 2.2.3. DTTR-TTA (3)

Compound 3 was obtained as a red solid (yield = 80%). Mp: 217 °C.  $^1\text{H}$  NMR (300 MHz,  $\text{CDCl}_3$ )  $\delta$ : 7.38 (s, 2H), 6.99 (s, 2H), 2.98 (t,  $J = 7.6$  Hz, 4H), 2.74 (t,  $J = 7.5$  Hz, 4 H), 1.79 (m, 8H), 1.27 (br, 64 H), 0.88 (m, 12H). This material was insufficiently soluble to obtain a  $^{13}\text{C}$  NMR spectrum. HRMS ( $m/z$ , FAB+) calcd for  $\text{C}_{70}\text{H}_{96}\text{S}_{10}$ , 1256.4719; found: 1256.4724.

**Device Fabrication and Characterization:** The pristine compounds 1–3 and DTTR-TT:PDIT-SBT blend films were solution-sheared from 2 mg  $\text{mL}^{-1}$  chlorobenzene solution onto Si/SiO<sub>2</sub> substrates modified with octadecyltrichlorosilane (ODTS). The details of the solution-shearing apparatus were summarized in a previous report.<sup>[65]</sup> Source and drain electrodes with a channel width/length ( $W/L$ ) of 1500 and 25  $\mu\text{m}$  were thermally evaporated through the metal mask. All the OFETs devices were measured in a  $\text{N}_2$ -filled atmosphere and recorded with a Keithley 4200-SCS semiconductor parameters analyzer and probe station at room temperature. The mobilities ( $\mu$ ) and threshold voltage ( $V_{\text{th}}$ ) are obtained from the slope and intercept of a plot of  $I_{\text{d}}$  against the  $V_{\text{g}}$ , using the following equation

$$I_{\text{d}} = \frac{W\mu C}{2L} (V_{\text{g}} - V_{\text{th}})^2 \quad (1)$$

where  $I_{\text{d}}$  is the drain current,  $V_{\text{g}}$  is the gate voltage, and  $C$  is capacitance per unit area of the gate dielectric layer.

## 3. Results and Discussion

The synthetic approach to DTTR compounds, DTTR-TT (1), DTTR-DTT (2), and DTTR-TTA (3), is presented in **Scheme 1**. Target compounds are synthesized by Stille coupling reaction between monobromodialkylthiophene (6) and distannylated units such as thienothiophene, dithienothiophene, and tetrathienoacene, respectively. Dialkylthiophene (5), monobromodialkylthiophene (6), and distannylated compounds were prepared according to procedures in the literature.<sup>[63,65]</sup> The new molecules were purified by recrystallization from toluene. The chemical structures of the final compounds were characterized by NMR, high-resolution mass spectroscopy, and elementary analysis. These newly synthesized compounds possess adequate solubility in the organic solvents. The thermal behaviors of these three samples were investigated by differential scanning calorimetry (DSC, Figure S2, Supporting Information) and thermogravimetric analysis (TGA, Figure S3, Supporting Information) under nitrogen atmosphere and the results summarized in **Table 1**.

The new fused thiophene-based compounds have good thermal stability and the TGA plots indicate that weight loss ( $\approx 5\%$ ) only occurs with heating above 375 °C. The DSC data reveal major endothermic melting peaks at 124, 121, and 220 °C for compounds 1–3, respectively. For the pure DTTR-TT solid, two main peaks at 74 and 124 °C were observed for crystal-liquid crystal phase transition and isotropization, respectively. The other two compounds do not appear to show the liquid crystal transition due to the stronger main chain interaction from the rigid backbone based on more extended  $\pi$ -conjugated fused thiophene ring in the central core. The absorption spectra in solution and thin films are depicted in **Figure 3** and the results are listed in Table 1. All three DTTR compounds in diluted *o*-dichlorobenzene solution exhibited strong absorption in the range of 350–500 nm, with maximum peaks located at 398, 411, and 423 nm for DTTR-TT, DTTR-DTT, and DTTR-TTA, respectively. It is clear that the increase in the fused thiophene units for the central core leads to the absorption being redshifted, which is likely attributed to the extended  $\pi$ -conjugation.<sup>[66]</sup> From solution to solid state, the absorption maximum of DTTR-TT, DTTR-DTT, and DTTR-TTA is bathochromically shifted. The strong shoulder peaks, especially for DTTR-TTA sample, as well as relatively large redshift suggest the aggregation tendency originated from intense interchain interaction between these  $\pi$ -conjugated molecules. Based on the onset thin

**Table 1.** Thermal, optical and electrochemical properties of three compounds.

Compounds	$T_{\text{d}}^{\text{a}}$ [°C]	$T_{\text{m}}^{\text{b}}$ [°C]	$\lambda_{\text{max}}^{\text{c}}$ [nm]	$E_{\text{g}}^{\text{d}}$ [eV]	$E_{\text{ox}}^{\text{e}}$ [V]	HOMO [eV]	LUMO [eV]		
DTTR-TT (1)	385	124	398	2.28	0.96	−5.16 <sup>f</sup>	−5.05 <sup>g</sup>	−2.88 <sup>h</sup>	−1.70 <sup>g</sup>
DTTR-DTT (2)	382	121	411	2.22	0.93	−5.13 <sup>f</sup>	−5.02 <sup>g</sup>	−2.91 <sup>h</sup>	−1.80 <sup>g</sup>
DTTR-TTA (3)	384	220	423	2.17	0.85	−5.05 <sup>f</sup>	−4.99 <sup>g</sup>	−2.88 <sup>h</sup>	−1.87 <sup>g</sup>

Obtained from: <sup>a</sup>)TGA; <sup>b</sup>)DSC; where  $T_{\text{d}}$  = decomposition temperature and  $T_{\text{m}}$  = melting temperature; <sup>c</sup>)in *o*-C<sub>6</sub>H<sub>4</sub>Cl<sub>2</sub>; <sup>d</sup>)optical energy gap was calculated using  $1240/\lambda_{\text{abs}}(\text{onset})$ ; <sup>e</sup>)by DPV in *o*-C<sub>6</sub>H<sub>4</sub>Cl<sub>2</sub> at 25 °C,  $E_{\text{ox}}$  = oxidative potential. All potentials reported are reference to an Fc/Fc<sup>+</sup> internal standard (at −4.8 V); <sup>f</sup>)using HOMO =  $-(4.2+E_{\text{ox}})$ ; <sup>g</sup>)by DFT calculation; <sup>h</sup>)estimated from LUMO = HOMO+ $E_{\text{g}}$ .

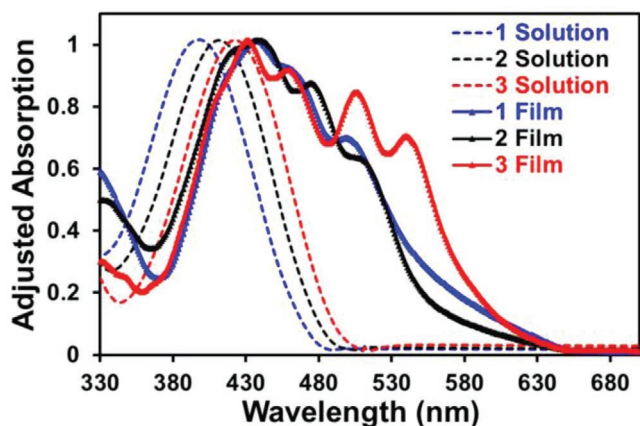


**Figure 3.** UV-vis absorption spectra of DTTR-TT (1), DTTR-DTT (2), and DTTR-TTA (3) in diluted solution (dotted line) and solution-sheared films (solid line).

film absorption, the optical bandgap ( $E_g$ ) is determined to be 2.28, 2.22, and 2.14 eV for DTTR-TT, DTTR-DTT, and DTTR-TTA, respectively, and the trend is in good agreement with the increased electron-donating ability from the extended fused thiophene core. In addition, the electrochemical properties of these three DTTR-based compounds were examined by solution differential pulse voltammetry (DPV) with a three-electrode configuration. All potentials reported are referenced to a  $Fc/Fc^+$  internal standard (calibrated at 0.6 V). The oxidation potentials ( $E_{ox}$ ) of DTTR-TT, DTTR-DTT, and DTTR-TTA are recorded at 0.96, 0.93, and 0.85 V (Figure 4a), respectively. The derived highest occupied molecular orbitals (HOMOs) of DTTR-TT, DTTR-DTT, and DTTR-TTA are thus estimated around  $-5.16$ ,  $-5.13$ , and  $-5.05$  eV, respectively, using the equation:  $E_{HOMO} = -(4.20 + E_{ox})$  eV, assuming  $Fc/Fc^+$  oxidation at  $-4.8$  eV. The upshifted HOMO level is mainly contributed by the extended fused thiophene rings, which may facilitate the hole injection and stabilize the generated organic cations. The lowest unoccupied molecular orbital (LUMO) energy level is calculated from the HOMO energy level and optical bandgap, using the equation:  $E_{LUMO} = E_{HOMO} + E_g$  and summarized in Table 1 and Figure 4b. Electronic structure calculations were performed at the B3LYP/6-31G\* level of density functional theory (DFT). The alkyl chains on DTTR moieties were omitted as the ethyl groups for computational simplicity. The electronic profiles of the calculated frontier molecular orbitals, DFT-derived HOMO

and LUMO values, and optimized molecular structures, as well as intramolecular dihedral angles, are shown in Figure S4 (Supporting Information) and summarized in Table 1. It was found that all three DTTR-based compounds have similar electron density distributions on HOMO and LUMO, and the electron densities are delocalized on the whole conjugated framework. The extension of conjugation on the end-capped fused thiophene ring system appears to lead to a further slight increase in the HOMO level and decrease in the LUMO level; therefore, DTTR-TTA exhibited the smallest energy gap among the studied series. In addition, the molecular calculations show there are noticeable differences in molecular planarity for the DTTR derivatives. As shown in Figure S4b (Supporting Information), the dihedral angles are less deviated in DTTR-TTA ( $46.4^\circ$ ) versus those in DTTR-DTT ( $48.2^\circ$ ) and DTTR-TT ( $49.3^\circ$ ), indicating better molecular conjugation and smaller energy gaps in DTTR-TTA, which is in good agreement with the electrochemically and optically derived data.

OFETs with bottom-gate top-contact (BGTC) device configuration (doped  $Si/SiO_2$ /self-assembly monolayer (SAM)/organic semiconductors (1–3)/Au) were fabricated to investigate the charge transport characteristics. ODTs was used as SAM. The 1–3 semiconducting layer was solution-sheared from chlorobenzene ( $2 \text{ mg mL}^{-1}$ ) onto the heated substrates ( $60\text{--}70^\circ\text{C}$ ). The sequential annealing was performed at  $50^\circ\text{C}$  for 3 h under vacuum. A gold electrode was deposited as the patterned source and drain contacts. OFETs fabrication and measurement details are included in the Experimental Section. Solution-shearing is a useful one-step solution processing technique which can fabricate crystalline film through the meniscus effect. Typical transfer and output curves of 1–3 OFETs devices are shown in Figure 5 and Figure S5 (Supporting Information), and all three small molecule semiconductors exhibited p-type transfer characteristics in the negative gate voltage ( $V_g$ ) region when measured in air. The assessed OFETs device performances, such as field effect mobility ( $\mu$ ), threshold voltage ( $V_{th}$ ), and ON/OFF current ratio ( $I_{ON}/I_{OFF}$ ), are shown in Table 2. It is noted that the mobility and threshold voltage were extracted from the slope and intercept of the square root of drain current ( $I_d$ ) versus gate voltage ( $V_g$ ) plot in the saturation region. Moderate hole mobilities in the range of  $10^{-4}\text{--}10^{-2} \text{ cm}^2 \text{ V}^{-1} \text{ s}^{-1}$  were observed for these three devices. The maximum mobilities ( $\mu_{max}$ ) are 0.0009, 0.0023, and  $0.016 \text{ cm}^2 \text{ V}^{-1} \text{ s}^{-1}$  for DTTR-TT, DTTR-DTT, and DTTR-TTA, respectively. Subsequent extraction of hole mobilities of DTTR-TT OFETs results in an average mobility ( $\mu_{avg}$ )

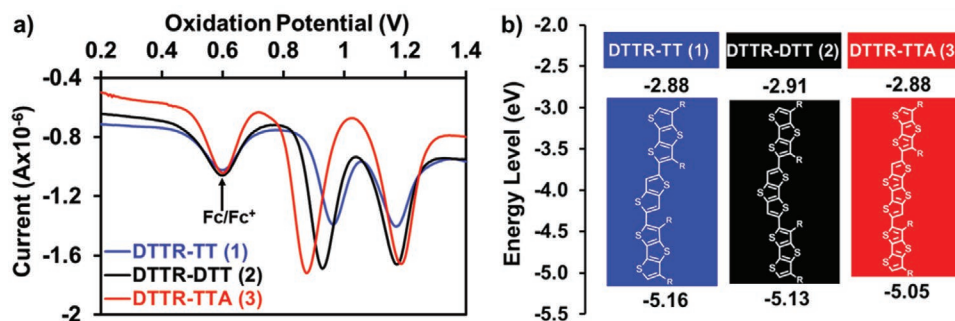


**Figure 4.** a) DPV curves of 1–3 in *o*-dichlorobenzene. b) Experimental HOMO and LUMO energy level.

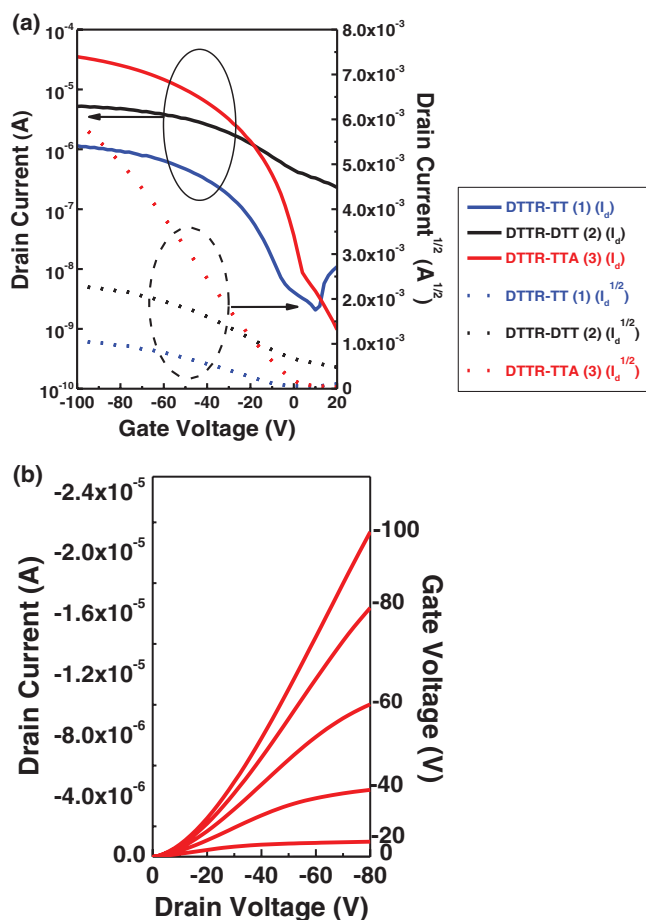


**Figure 5.** a) Representative transfer characteristics of solution-sheared OFETs based on all three compounds thin films. b) Output characteristics of solution-sheared OFETs based on DTTR-TTA film.

of  $(0.0003 \pm 0.0002) \text{ cm}^2 \text{ V}^{-1} \text{ s}^{-1}$  across 15 devices, compared to  $(0.0018 \pm 0.0005)$  and  $(0.013 \pm 0.002) \text{ cm}^2 \text{ V}^{-1} \text{ s}^{-1}$  for DTTR-DTT and DTTR-TTA, with the errors ascribed to these mean values being the estimated standard deviation of the distribution. Overall, DTTR-TTA OFETs present the highest  $I_{\text{ON}}/I_{\text{OFF}}$  of  $10^4$ – $10^5$  and enhanced mobilities of  $\approx 10$ - and 100-fold in comparison to DTTR-TT and DTTR-DTT, respectively. The observed higher hole mobilities in DTTR-TTA are mainly due to more  $\pi$ -extended conjugation and stronger intermolecular interaction. Besides the frontier molecular orbitals, the thin film morphologies and microstructural data were strongly influenced by the size of the  $\pi$ -conjugated fused thiophene core with both ends capped by the DIT group, which also plays an important role in dictating the charge transport properties. The surface morphologies of the compound 1–3 film were investigated

**Table 2.** Summary of OFET parameters of small molecules 1–3.

Compounds	$\mu_{\text{max}}$ [ $\text{cm}^2 \text{ V}^{-1} \text{ s}^{-1}$ ]	$\mu_{\text{avg}}$ [ $\text{cm}^2 \text{ V}^{-1} \text{ s}^{-1}$ ]	$I_{\text{ON}}/I_{\text{OFF}}$ (-)	$V_{\text{th}}$ [V]
DTTR-TT (1)	0.0009	$0.0003 \pm 0.0002$	$10^2$ – $10^3$	$-8.4 \pm 1.0$
DTTR-DTT (2)	0.0023	$0.0018 \pm 0.0005$	$10^2$ – $10^3$	$27.2 \pm 13.7$
DTTR-TTA (3)	0.016	$0.013 \pm 0.002$	$10^4$ – $10^5$	$-10.1 \pm 4.3$

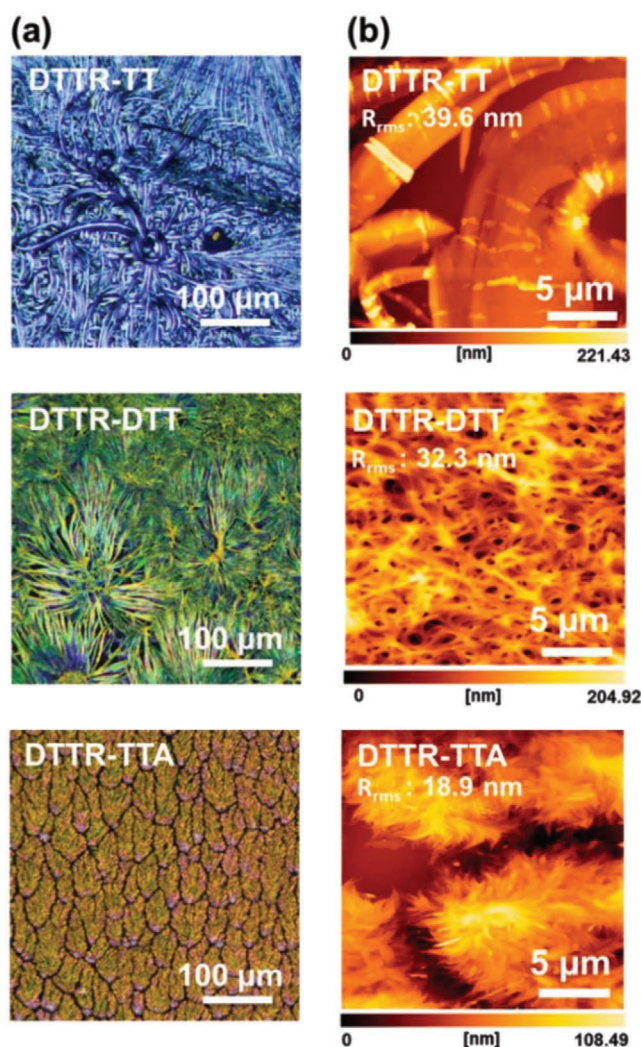


**Figure 6.** a) POM and b) AFM images of solution-sheared DTTR-TT, DTTR-DTT, and DTTR-TTA thin films.

by POM (Figure 6a) and atomic force microscopy (AFM) (Figure 6b), where the solution-sheared condition and substrate modification used for imaging are the same as those for the fabricated active layer in the OFETs device. POM images reveal nonoriented distinctive fibrillar-like grains with some voids for DTTR-TT and DTTR-DTT films, whereas the DTTR-TTA film exhibits larger and more compact aggregated domains. Furthermore, the surface morphologies of solution-sheared film are investigated by tapping mode AFM. The extended  $\pi$ -conjugated central core in DTTR-TTA also causes the formation of the large crystal domains. These observed morphologies in POM and AFM indicate that DTTR-TTA possesses strong intermolecular interaction upon thin film processing. Besides, the resulting height images reveal that the DTTR-TTA thin film has flat morphologies with a smaller root-mean-square roughness ( $R_{\text{rms}}$ ), meaning the relatively reduced grain boundaries formed with effective molecular assemblies.

We then probed the microstructural formation using 2D grazing incidence X-ray diffraction (GIXRD; Figure S6, Supporting Information). All three films with lamellar scattering in

the out-of-plane ( $q_z$ ) direction indicate an edge-on dominating orientation. The solution-sheared DTTR-TTA thin film displays a higher degree of diffraction spots (up to four orders) in a  $q_z$  orientation, suggesting the formation of more highly ordered lamellar packing. An approximately isotropic alignment was observed, as evidenced by the dot-like (00 $l$ ) peaks in the pattern. These characteristics can explain the highest mobilities in the DTTR-TTA thin film. Although our newly synthesized small molecule semiconductors tend to aggregate at microscopic levels due to the strong molecular interaction, the discontinuous crystal with voids and grain boundaries negatively affects the charge carrier transport within the film. Mixtures of small molecules with conjugated polymers which function as a matrix or binder allow greater control over film formation and microstructural engineering, which is probably beneficial for efficient charge transport as compared with the single components. Therefore, we evaluate the structural changes in the lowest mobility of DTTR-TT films to improve the charge transport properties by blending with PDTT-SBT polymers. It is noted here that X% blend comprises a weight ratio of X% DTTR-TT small molecules in the blend films. The DSC experiments were performed to primarily analyze the phase transitions of pure DTTR-TT and its blend upon heating (Figure S7, Supporting Information). These two thermal transition temperatures fall to 71 and 105 °C for the DTTR-TT:PDTT-SBT blend (50%) as compared with the pure DTTR-TT. The decrease in transition temperatures according to the colligative property reflects the intermingling of these two compounds while retaining good crystallinity. The molecular interactions in the DTTR-TT:PDTT-SBT blend film were also spectroscopy reflected by their absorption behavior (Figure S8, Supporting Information). The blend films display a similar absorption position with a dual band in the range of 350–500 and 500–700 nm, originated from the absorption features of DTTR-TT and PDTT-SBT, respectively. Absorption in a higher wavelength region increases upon the addition of PDTT-SBT, accompanied by a decrease in lower wavelength absorption. No additional change of absorption band was detected within 350–700 nm. Therefore, these absorption bands are probably contributed by the formation of PDTT-SBT agglomerates in the presence of DTTR-TT crystals.

To further assess the impact of the composition of blend film on the charge transfer properties, DTTR-TT:PDTT-SBT blends were further investigated by their implementation as semiconducting channels in OFETs. Therefore, 15 OFETs for each blend were measured to give a broader statistical image of the effects of blend composition on performance. Figures S9–S18 (Supporting Information) illustrate a set of representative transfer characteristics recorded at saturation ( $V_d = -100$  V) and the output characteristic of the blend channel with various DTTR-TT ratios from 0% to 100%, whereas numerical information on the device results can be found in **Table 3** and graphically in **Figure 7** to give a clear idea of the parameters' spread and how the trends of each parameter develop with blend composition. All the blend OFETs clearly show unipolar and hysteresis-less p-type charge transport characteristics which are strongly determined by the composition of the semiconducting blend film. The hole mobility of the 100% blend (pristine DTTR-TT) was found to be modest ( $10^{-4}$ – $10^{-3}$  cm<sup>2</sup> V<sup>-1</sup> s<sup>-1</sup>) with a lower  $V_{th}$  of  $-8.4 \pm 1.0$  V, whereas the 0% blend (pristine PDTT-SBT) devices

**Table 3.** Summary of OFET parameters based on DTTR-TT:PDTT-SBT blend thin films.

DTTR-TT composition in blend [%]	$\mu_{max}$ [cm <sup>2</sup> V <sup>-1</sup> s <sup>-1</sup> ]	$\mu_{avg}$ [cm <sup>2</sup> V <sup>-1</sup> s <sup>-1</sup> ]	$I_{ON}/I_{OFF}$ (-)	$V_{th}$ [V]
0	0.067	$0.039 \pm 0.019$	$4.7 \times 10^4$	$-35.1 \pm 5.3$
10	0.049	$0.022 \pm 0.012$	$9.3 \times 10^4$	$-32.4 \pm 2.2$
20	0.086	$0.069 \pm 0.011$	$1.8 \times 10^5$	$-26.3 \pm 4.6$
30	0.22	$0.11 \pm 0.04$	$2.0 \times 10^5$	$-21.5 \pm 4.9$
40	0.077	$0.043 \pm 0.016$	$3.6 \times 10^4$	$-20.6 \pm 2.9$
50	0.087	$0.052 \pm 0.021$	$1.8 \times 10^5$	$-17.8 \pm 4.2$
60	0.088	$0.049 \pm 0.024$	$3.3 \times 10^4$	$-13.1 \pm 2.1$
70	0.039	$0.026 \pm 0.012$	$1.6 \times 10^4$	$-12.1 \pm 3.8$
80	0.026	$0.019 \pm 0.006$	$1.1 \times 10^4$	$-3.9 \pm 5.2$
90	0.070	$0.041 \pm 0.026$	$1.6 \times 10^4$	$-1.7 \pm 4.5$
100	0.0009	$0.0003 \pm 0.0002$	$1.1 \times 10^2$	$-8.4 \pm 1.0$

yield the  $\mu_{max}$  and  $\mu_{avg}$  of 0.067 and  $0.039 \pm 0.019$  cm<sup>2</sup> V<sup>-1</sup> s<sup>-1</sup> with a larger  $V_{th}$  of  $-35.1 \pm 5.3$  V, as expected from the literature.<sup>[62]</sup> Under the same fabrication conditions, the DTTR-TT:PDTT-SBT blends yield  $\mu_{max}$  ( $\mu_{avg}$ ) between 0.0009 ( $0.0003 \pm 0.0002$ ) and 0.22 ( $0.11 \pm 0.04$ ) cm<sup>2</sup> V<sup>-1</sup> s<sup>-1</sup>. There is a clear rising trend occurring in the mobilities upon addition of the PDTT-SBT polymer. Upon addition of a small quantity of PDTT-SBT polymer (10%), the hole mobility in these blend devices increases sharply, with the change from pristine DTTR-TT (100% blend) to 90% blend causing two orders of magnitude improvement in saturation mobilities. Blend OFETs comprising 30% DTTR-TT in the active layer exhibit the most pronounced improvement in the mobility, with the order up to  $10^{-1}$  cm<sup>2</sup> V<sup>-1</sup> s<sup>-1</sup>, which is almost three times higher than pristine PDTT-SBT. Additionally, the  $V_{th}$  of blend films increases from  $-1.7 \pm 4.5$  V (90% blend) to  $-35.1 \pm 5.3$  V (0% blend) as the DTTR-TT loading decreases, shifting far away from 0 V.

The surface morphologies of DTTR-TT:PDTT-SBT blend films were characterized by POM and AFM, where the

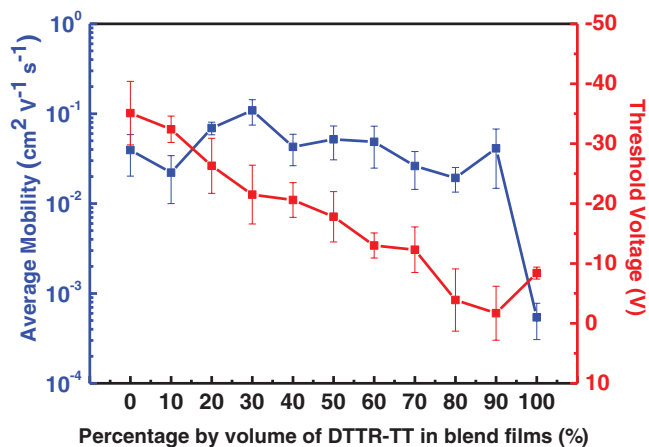


**Figure 7.** Average mobilities and threshold voltage of blend OFETs as a function of X% DTTR-TT in blend films.

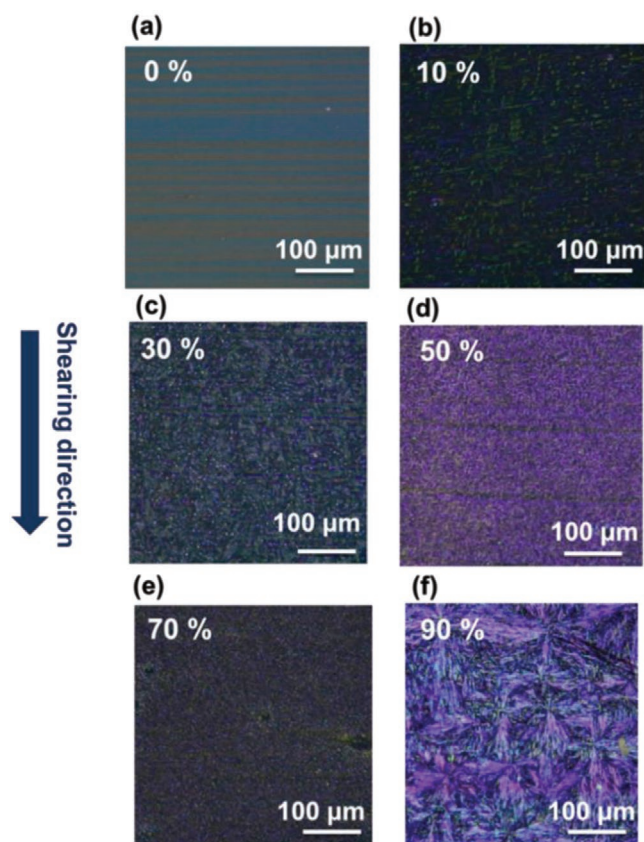


**Figure 8.** a–f) POM images of solution-sheared 0%, 10%, 30%, 50%, 70%, and 90% blend thin film, respectively.

processing parameters are the same as those for active layer film in OFETs. **Figure 8a–f** shows the POM images of DTTR-TT:PDTT-SBT blend at 0%, 10%, 30%, 50%, 70%, and 90%, respectively, and those for other blend compositions are shown in Figure S19 (Supporting Information). The pristine PDTT-SBT (0% blend) film does not exhibit any obvious crystals along the shearing direction (Figure 8a). However, the line-shaped domain perpendicular to the shearing direction is the thicker part in the film, which may be caused by the slow solvent evaporation during the shearing process. Starting from the 30% blend, a high density of small crystalline agglomerates were distributed within all the blend films and more obvious agglomerates can be observed with a higher DTTR-TT loading concentration. In the 100% blend film (pristine DTTR-TT; Figure 6a), separated fibrillar-like grains are found. In addition, from the tapping mode AFM image in Figure S20 (Supporting Information), poor grain connectivity can be found in the pristine DTTR-TT (100% blend) film (Figure 6b) even though the morphologies of the grain changes dramatically with the randomly grown large ribbon-shaped structure. The sharp grain boundaries may limit the charge transport within the DTTR-TT film. It is also clear from the AFM image (Figure S20a, Supporting Information) that a nontextured and featureless surface in pristine PDTT-SBT (0% blend) film is formed on the substrate. By blending of these two materials, fibrillar-like features start to appear and progressively increase in size as the DTTR-TT weight ratio increases. The images suggest that the

DTTR-TT:PDTT-SBT blend films are composed of DTTR-TT agglomerates distributed in the PDTT-SBT matrix<sup>[47]</sup> or vertically separated by the bottom PDTT-SBT layer.<sup>[49]</sup> The blend film with 10% DTTR-TT loading shows fragmented fibril bundles, whereas the microstructural organization of the DTTR-TT small molecules percolate uniformly in the 30% blend film with a dense network of a fibrillar crystals. Increasing the DTTR-TT further to 50% (Figure S20d, Supporting Information) and 70% (Figure S20e, Supporting Information) blends, the strong  $\pi$ - $\pi$  interaction between the small molecules contributes to the aggregation into larger fibrillar crystals, which are more clearly visible with separated grains. It is worth noting that the intertwined and long-range fibrillar structures in the 30% (Figure S20c, Supporting Information) DTTR-TT:PDTT-SBT blend provide good semiconducting percolation between the crystals (mainly from the DTTR-TT domain) in the interconnected network (from the long PDTT-SBT chain, which may be very useful for improving charge transport properties). The crystalline nature and molecular packing of solution-sheared blend film containing DTTR-TT at 0%, 30%, 50, 70%, and 100% were investigated by 2D GIXRD to correlate with the OFET performance, with the results shown in **Figure 9**. The pristine PDTT-SBT (0% blend) film exhibits a (100) lamellar stacking diffraction peak (arrow in blue; Figure 9a) in the  $q_z$  direction with a  $d$ -spacing of 21.2 Å. It is clear that the pristine PDTT-SBT film has relatively low crystallinity, which is evidenced by the absence of a higher lamellar peak and low intensity obtained from the 1D scattering profile. On the other hand, the pristine DTTR-TT (100% blend) exhibits the corresponding arc-shaped lamellar diffraction patterns (arrows in red; Figure 9e), which suggests the DTTR-TT with has a large orientation and weak alignment with respect to the substrate. In the case of blend films, all the blend compositions investigated (30%, 50%, and 70%) exhibit GIXRD diffraction (Figure 9b–d) corresponding to the sums of patterns from PDTT-SBT (arrows in blue) and DTTR-TT (arrows in red) pure components. The value for out-of-plane scattering peaks and their corresponding  $d$ -spacing for any of blend films are similar to those observed for neat samples. These suggest that blending PDTT-SBT polymer with DTTR-TT does not alter the packing of these blend molecules in their crystalline phase. Besides, the addition of DTTR-TT in the blend films leads to an increase in the sharp the (001) peak intensity (Figure S21, Supporting Information), assigned from the DTTR-TT crystalline fraction. The azimuthal scattering profiles as a function of blend composition at various ranges of azimuthal angles were also taken from the (001) diffractions in the 2D GIXRD pattern of the DTTR-TT:PDTT-SBT blend films (Figure S22, Supporting Information). The narrowest peak full width at half maximum (FWHM) at around the 30% DTTR-TT composition in blend shows a larger fraction of the aligned crystalline domains, and the data suggest that non-oriented crystal growth increases as the amount of DTTR-TT rises, due to the increased peak FWHM in Figure S22 (Supporting Information) and more arc-like diffraction pattern in Figure 9e. From the discussion above, a synergistic balance between the degree of crystallinity and molecular ordering can help the 30% blend films obtain improved macroscopic charge transport properties. The observation of the GIXRD diffraction as a function of blend composition shows that the mixing of



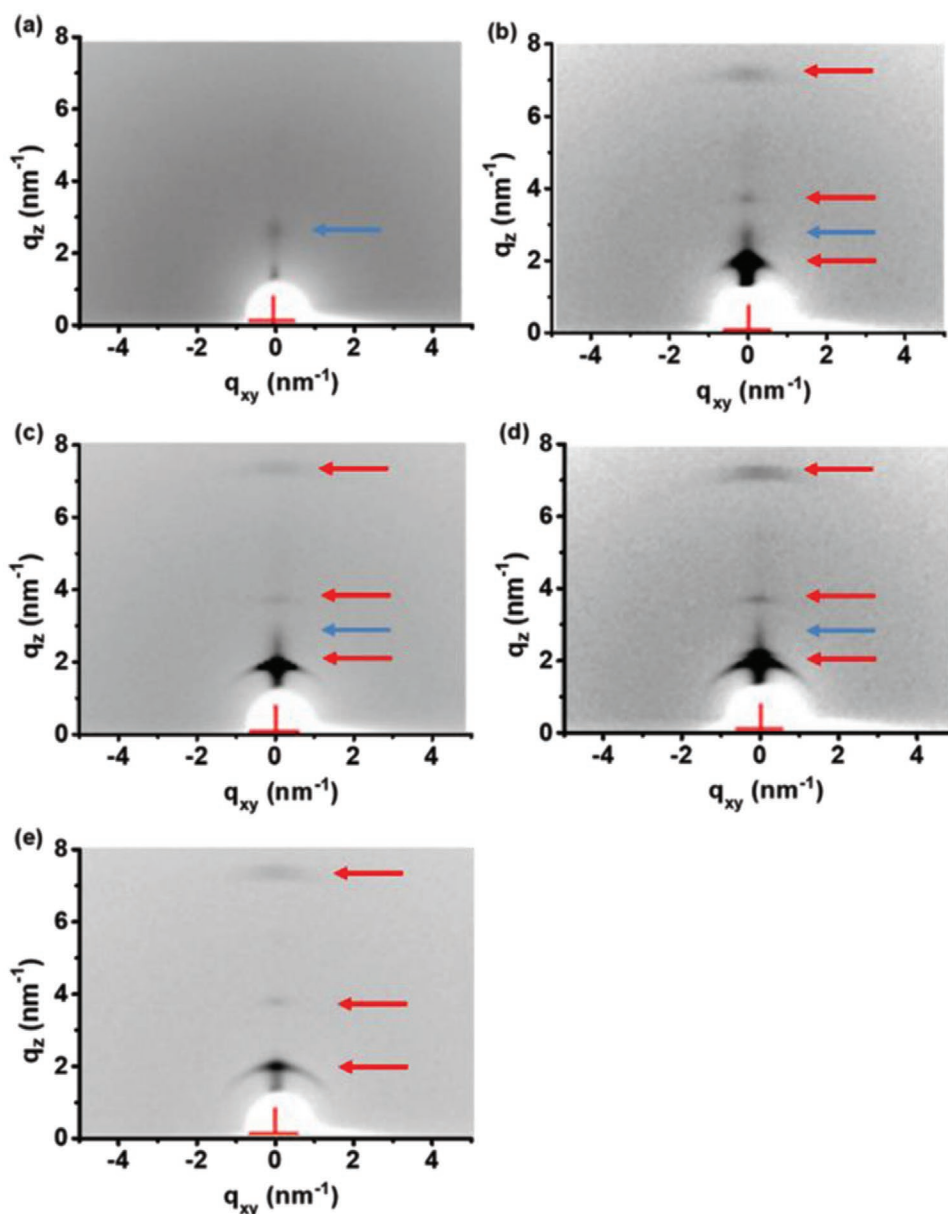


**Figure 9.** a–e) 2D GIXRD patterns of solution-sheared 0%, 30%, 50%, 70%, and 100% blend thin films, respectively.

PDTT-SBT polymer influences both the blend film crystallinity and microstructure.

It can be concluded here that the positive effects of PDTT-SBT on the crystallization of DTTR-TT can be attributed to two factors. First, PDTT-SBT serves as a nucleating agent that provides the heterogeneous nucleation sites to accelerate the crystallization of DTTR-TT in the blend during the shearing process. This can be verified by the DSC profiles in Figure S7 (Supporting Information) where the 50% blend shows a higher crystallinity of DTTR-TT than that of pure DTTR-TT. Second, the long polymer chains of PDTT-SBT tend to be extended and oriented under shearing, which in turn causes an alignment of the DTTR-TT crystallites nucleated on the PDTT-SBT chains. Among the blends, the composition of the 30% one happens to be optimal for the formation of continuous and oriented

DTTR-TT crystal domains, as confirmed by the AFM image (Figure S20, Supporting Information) and GIXRD pattern (Figure 9). This explains why the 30% blend shows the highest hole mobility.

#### 4. Conclusion

In conclusion, three conjugated multifused thiophene small molecular semiconductors with modification of central core (DTTR-TT, DTTR-DTT, and DTTR-TTA) were synthesized, and their suitability with regard to p-type OFETs was studied. The selection of different central fused thiophene core groups can significantly alter the backbone conformation of the resulting small molecules, which further impacts the frontier molecular

orbitals and assembly properties, eventually influencing their morphologies/microstructures and electrical semiconducting characteristics. Among all the materials studied, DTTR-TTA contains the most expanded  $\pi$ -conjugated central core, four fused thiophene (TTA), exhibited the best OFETs performance with hole mobilities of ca.  $0.016 \text{ cm}^2 \text{ V}^{-1} \text{ s}^{-1}$ . Meanwhile, a substantial change in electrical properties from a mixture of DTTR-TT with PDTT-SBT polymer was also examined as a function of blend composition. The optimized features from crystalline DTTR-TT and ordered PDTT-SBT were organized into the morphologies with DTTR-TT crystal embedded at interconnected PDTT-SBT domain, occurring at 30% DTTR-TT in blend. The 30% blend OFETs exhibited the highest mobility of  $0.22 \text{ cm}^2 \text{ V}^{-1} \text{ s}^{-1}$ , which is 250 and 3 times higher than that of pristine DTTR-TT ( $0.0009 \text{ cm}^2 \text{ V}^{-1} \text{ s}^{-1}$ ) and PDTT-SBT ( $0.067 \text{ cm}^2 \text{ V}^{-1} \text{ s}^{-1}$ ), respectively. We reported an efficient strategy to improve the mobility of small molecule DTTR-TT from  $0.0009$  to  $0.22 \text{ cm}^2 \text{ V}^{-1} \text{ s}^{-1}$  by blending with easily synthesizable PDTT-SBT polymer. Our findings help to establish the structure–property relationships in solution-processed multifused thiophene-based small molecule semiconductors with a polymer blend and can help in exploring tunable molecular interaction.

## Supporting Information

Supporting Information is available from the Wiley Online Library or from the author.

## Acknowledgements

S.N.A. and G.-Y.H. contributed equally to this work. This work was supported by the Ministry of Science and Technology (MOST) in Taiwan. C.-L.L. gratefully acknowledges the funding from the Young Scholar Fellowship Program (Columbus Program) by MOST in Taiwan, under Grant MOST 109-2636-E-002-029. M.-C.C. thanks the funding provided by MOST (MOST 109-3111-8-008-001) and NCU-DSM Research Center. The authors thank Beamline B13A1/B17A1/B23A1 from the National Synchrotron Radiation Research Center (NSRRC) of Taiwan for providing beamtime.

## Conflict of Interest

The authors declare no conflict of interest.

## Keywords

organic field effect transistors, organic semiconductors, polymer blend, soluble dithienothiophenes, solution process

Received: October 15, 2020

Revised: December 5, 2020

Published online: February 10, 2021

[1] T. Okamoto, C. P. Yu, C. Mitsui, M. Yamagishi, H. Ishii, J. Takeya, *J. Am. Chem. Soc.* **2020**, *142*, 9083.

[2] J. Yang, Z. Zhao, S. Wang, Y. Guo, Y. Liu, *Chem* **2018**, *4*, 2748.

- [3] M. Kim, S. U. Ryu, S. A. Park, K. Choi, T. Kim, D. Chung, T. Park, *Adv. Funct. Mater.* **2020**, *30*, 1904545.
- [4] Q. Liu, S. E. Bottle, P. Sonar, *Adv. Mater.* **2020**, *32*, 1903882.
- [5] A. Wadsworth, H. Chen, K. J. Thorley, C. Cendra, M. Nikolka, H. Bristow, M. Moser, A. Salleo, T. D. Anthopoulos, H. Sirringhaus, I. McCulloch, *J. Am. Chem. Soc.* **2020**, *142*, 652.
- [6] U. Zschieschang, H. Klauk, *J. Mater. Chem. C* **2019**, *7*, 5522.
- [7] C.-A. Di, H. Shen, F. Zhang, D. Zhu, *Acc. Chem. Res.* **2019**, *52*, 1113.
- [8] W. Tang, Y. Huang, L. Han, R. Liu, Y. Su, X. Guo, F. Yan, *J. Mater. Chem. C* **2019**, *7*, 790.
- [9] D. Khim, A. Luzio, G. E. Bonacchini, G. Pace, M.-J. Lee, Y.-Y. Noh, M. Caironi, *Adv. Mater.* **2018**, *30*, 1705463.
- [10] J. T. E. Quinn, J. Zhu, X. Li, J. Wang, Y. Li, *J. Mater. Chem. C* **2017**, *5*, 8654.
- [11] L. J. Richter, D. M. DeLongchamp, A. Amassian, *Chem. Rev.* **2017**, *117*, 6332.
- [12] Y. Lyu, D. Cui, J. Huang, W. Fan, Y. Miao, K. Pu, *Angew. Chem., Int. Ed.* **2019**, *58*, 4983.
- [13] S. Nam, S. G. Hahm, D. Khim, H. Kim, T. Sajoto, M. Ree, S. R. Marder, T. D. Anthopoulos, D. D. C. Bradley, Y. Kim, *ACS Appl. Mater. Interfaces* **2018**, *10*, 12921.
- [14] H. Yan, Z. Chen, Y. Zheng, C. Newman, J. R. Quinn, F. Dötz, M. Kastler, A. Facchetti, *Nature* **2009**, *457*, 679.
- [15] L. Zhang, N. S. Colella, B. P. Cherniawski, S. C. B. Mannsfeld, A. L. Briseno, *ACS Appl. Mater. Interfaces* **2014**, *6*, 5327.
- [16] K. Takimiya, M. Nakano, H. Sugino, I. Osaka, *Synth. Met.* **2016**, *217*, 68.
- [17] A. N. Lakshminarayana, A. Ong, C. Chi, *J. Mater. Chem. C* **2018**, *6*, 3551.
- [18] M. Chen, L. Yan, Y. Zhao, I. Murtaza, H. Meng, W. Huang, *J. Mater. Chem. C* **2018**, *6*, 7416.
- [19] W. Jiang, Y. Li, Z. Wang, *Chem. Soc. Rev.* **2013**, *42*, 6113.
- [20] Y. M. Sun, Y. Q. Ma, Y. Q. Liu, Y. Y. Lin, Z. Y. Wang, Y. Wang, C. A. Di, K. Xiao, X. M. Chen, W. F. Qiu, B. Zhang, G. Yu, W. P. Hu, D. B. Zhu, *Adv. Funct. Mater.* **2006**, *16*, 426.
- [21] P.-Y. Huang, L.-H. Chen, Y.-Y. Chen, W.-J. Chang, J.-J. Wang, K.-H. Lii, J.-Y. Yan, J.-C. Ho, C.-C. Lee, C. Kim, M.-C. Chen, *Chem. - Eur. J.* **2013**, *19*, 3721.
- [22] P.-Y. Huang, L.-H. Chen, C. Kim, H.-C. Chang, Y.-j. Liang, C.-Y. Feng, C.-M. Yeh, J.-C. Ho, C.-C. Lee, M.-C. Chen, *ACS Appl. Mater. Interfaces* **2012**, *4*, 6992.
- [23] N. Zhou, K. Prabakaran, B. Lee, S. H. Chang, B. Harutyunyan, P. Guo, M. R. Butler, A. Timalina, M. J. Bedzyk, M. A. Ratner, S. Vegiraju, S. Yau, C.-G. Wu, R. P. H. Chang, A. Facchetti, M.-C. Chen, T. J. Marks, *J. Am. Chem. Soc.* **2015**, *137*, 4414.
- [24] S.-S. Cheng, P.-Y. Huang, M. Ramesh, H.-C. Chang, L.-M. Chen, C.-M. Yeh, C.-L. Fung, M.-C. Wu, C.-C. Liu, C. Kim, H.-C. Lin, M.-C. Chen, C.-W. Chu, *Adv. Funct. Mater.* **2014**, *24*, 2057.
- [25] N. Zhou, S. Vegiraju, X. Yu, E. F. Manley, M. R. Butler, M. J. Leonard, P. Guo, W. Zhao, Y. Hu, K. Prabakaran, R. P. H. Chang, M. A. Ratner, L. X. Chen, A. Facchetti, M.-C. Chen, T. J. Marks, *J. Mater. Chem. C* **2015**, *3*, 8932.
- [26] K. Xiao, Y. Liu, T. Qi, W. Zhang, F. Wang, J. Gao, W. Qiu, Y. Ma, G. Cui, S. Chen, X. Zhan, G. Yu, J. Qin, W. Hu, D. Zhu, *J. Am. Chem. Soc.* **2005**, *127*, 13281.
- [27] J. Youn, P.-Y. Huang, Y.-W. Huang, M.-C. Chen, Y.-J. Lin, H. Huang, R. P. Ortiz, C. Stern, M.-C. Chung, C.-Y. Feng, L.-H. Chen, A. Facchetti, T. J. Marks, *Adv. Funct. Mater.* **2012**, *22*, 48.
- [28] S. Vegiraju, X.-L. Luo, L.-H. Li, S. N. Afraj, C. Lee, D. Zheng, H.-C. Hsieh, C.-C. Lin, S.-H. Hong, H.-C. Tsai, G.-H. Lee, S.-H. Tung, C.-L. Liu, M.-C. Chen, A. Facchetti, *Chem. Mater.* **2020**, *32*, 1422.
- [29] Z. Xue, S. Chen, N. Gao, Y. Xue, B. Lu, O. A. Watson, L. Zang, J. Xu, *Polym. Rev.* **2020**, *60*, 318.
- [30] G. Turkoglu, M. E. Cinar, T. Ozturk, *Top. Curr. Chem.* **2017**, *375*, 84.

- [31] S. Vegiraju, D.-Y. Huang, P. Priyanka, Y.-S. Li, X.-L. Luo, S.-H. Hong, J.-S. Ni, S.-H. Tung, C.-L. Wang, W.-C. Lien, S. L. Yau, C.-L. Liu, M.-C. Chen, *Chem. Commun.* **2017**, 53, 5898.
- [32] S. Vegiraju, C.-Y. Lin, P. Priyanka, D.-Y. Huang, X.-L. Luo, H.-C. Tsai, S.-H. Hong, C.-J. Yeh, W.-C. Lien, C.-L. Wang, S.-H. Tung, C.-L. Liu, M.-C. Chen, A. Facchetti, *Adv. Funct. Mater.* **2018**, 28, 1801025.
- [33] M.-C. Chen, Y.-J. Chiang, C. Kim, Y.-J. Guo, S.-Y. Chen, Y.-J. Liang, Y.-W. Huang, T.-S. Hu, G.-H. Lee, A. Facchetti, T. J. Marks, *Chem. Commun.* **2009**, 1846.
- [34] W. Tang, S. P. Singh, K. H. Ong, Z.-K. Chen, *J. Mater. Chem.* **2010**, 20, 1497.
- [35] C. Lu, W.-C. Chen, *Chem. Asian J.* **2013**, 8, 2813.
- [36] N. C. Mamillapalli, S. Vegiraju, P. Priyanka, C.-Y. Lin, X.-L. Luo, H.-C. Tsai, S.-H. Hong, J.-S. Ni, W.-C. Lien, G. Kwon, S. L. Yau, C. Kim, C.-L. Liu, M.-C. Chen, *Dyes Pigm.* **2017**, 145, 584.
- [37] Y. Ezhumalai, B. Lee, M.-S. Fan, B. Harutyunyan, K. Prabakaran, C.-P. Lee, S. H. Chang, J.-S. Ni, S. Vegiraju, P. Priyanka, Y.-W. Wu, C.-W. Liu, S. Yau, J. T. Lin, C.-G. Wu, M. J. Bedzyk, R. P. H. Chang, M.-C. Chen, K.-C. Ho, T. J. Marks, *J. Mater. Chem. A* **2017**, 5, 12310.
- [38] B. Kang, F. Ge, L. Qiu, K. Cho, *Adv. Electron. Mater.* **2017**, 3, 1600240.
- [39] J. Smith, R. Hamilton, I. McCulloch, N. Stingelin-Stutzmann, M. Heeney, D. D. C. Bradley, T. D. Anthopoulos, *J. Mater. Chem.* **2010**, 20, 2562.
- [40] A. D. Scaccabarozzi, N. Stingelin, *J. Mater. Chem. A* **2014**, 2, 10818.
- [41] S. Riera-Galindo, F. Leonardi, R. Pfattner, M. Mas-Torrent, *Adv. Mater. Technol.* **2019**, 4, 1900104.
- [42] L.-H. Chou, Y. Na, C.-H. Park, M. S. Park, I. Osaka, F. S. Kim, C.-L. Liu, *Polymer* **2020**, 191, 122208.
- [43] D. K. Hwang, C. Fuentes-Hernandez, J. D. Berrigan, Y. Fang, J. Kim, W. J. Potscavage, H. Cheun, K. H. Sandhage, B. Kippelen, *J. Mater. Chem.* **2012**, 22, 5531.
- [44] D. Guo, T. Miyadera, S. Ikeda, T. Shimada, K. Saiki, *J. Appl. Phys.* **2007**, 102, 023706.
- [45] E. Orgiu, A. M. Masillamani, J.-O. Vogel, E. Treossi, A. Kiersnowski, M. Kastler, W. Pisula, F. Dötz, V. Palermo, P. Samorì, *Chem. Commun.* **2012**, 48, 1562.
- [46] L. Zhang, N. S. Colella, F. Liu, S. Trahan, J. K. Baral, H. H. Winter, S. C. B. Mannsfeld, A. L. Briseno, *J. Am. Chem. Soc.* **2013**, 135, 844.
- [47] P.-H. Chu, L. Zhang, N. S. Colella, B. Fu, J. O. Park, M. Srinivasarao, A. L. Briseño, E. Reichmanis, *ACS Appl. Mater. Interfaces* **2015**, 7, 6652.
- [48] D. M. Russell, C. J. Newsome, S. P. Li, T. Kugler, M. Ishida, T. Shimoda, *Appl. Phys. Lett.* **2005**, 87, 222109.
- [49] A. F. Paterson, N. D. Treat, W. Zhang, Z. Fei, G. Wyatt-Moon, H. Faber, G. Vourlias, P. A. Patsalas, O. Solomeshch, N. Tessler, M. Heeney, T. D. Anthopoulos, *Adv. Mater.* **2016**, 28, 7791.
- [50] R. Hamilton, J. Smith, S. Ogier, M. Heeney, J. E. Anthony, I. McCulloch, J. Veres, D. D. C. Bradley, T. D. Anthopoulos, *Adv. Mater.* **2009**, 21, 1166.
- [51] J. Smith, W. Zhang, R. Sougrat, K. Zhao, R. Li, D. Cha, A. Amassian, M. Heeney, I. McCulloch, T. D. Anthopoulos, *Adv. Mater.* **2012**, 24, 2441.
- [52] B. H. Wunsch, K. Kim, Y. Rho, B. Ahn, S. Jung, L. E. Polander, D. G. Bucknall, S. R. Marder, M. Ree, *J. Mater. Chem. C* **2013**, 1, 778.
- [53] S. B. Lee, B. Kang, D. Kim, C. Park, S. Kim, M. Lee, W. B. Lee, K. Cho, *ACS Appl. Mater. Interfaces* **2019**, 11, 47153.
- [54] J. Kang, N. Shin, D. Y. Jang, V. M. Prabhu, D. Y. Yoon, *J. Am. Chem. Soc.* **2008**, 130, 12273.
- [55] S. Subramanian, S. K. Park, S. R. Parkin, V. Podzorov, T. N. Jackson, J. E. Anthony, *J. Am. Chem. Soc.* **2008**, 130, 2706.
- [56] H. Ebata, T. Izawa, E. Miyazaki, K. Takimiya, M. Ikeda, H. Kuwabara, T. Yui, *J. Am. Chem. Soc.* **2007**, 129, 15732.
- [57] J. Panidi, A. F. Paterson, D. Khim, Z. Fei, Y. Han, L. Tsetseris, G. Vourlias, P. A. Patsalas, M. Heeney, T. D. Anthopoulos, *Adv. Sci.* **2018**, 5, 1700290.
- [58] A. F. Paterson, Y.-H. Lin, A. D. Mottram, Z. Fei, M. R. Niazi, A. R. Kirmani, A. Amassian, O. Solomeshch, N. Tessler, M. Heeney, T. D. Anthopoulos, *Adv. Electron. Mater.* **2018**, 4, 1700464.
- [59] B. S. Hunter, J. W. Ward, M. M. Payne, J. E. Anthony, O. D. Jurchescu, T. D. Anthopoulos, *Appl. Phys. Lett.* **2015**, 106, 223304.
- [60] K. Zhao, O. Wodo, D. Ren, H. U. Khan, M. R. Niazi, H. Hu, M. Abdelsamie, R. Li, E. Q. Li, L. Yu, B. Yan, M. M. Payne, J. Smith, J. E. Anthony, T. D. Anthopoulos, S. T. Thoroddsen, B. Ganapathysubramanian, A. Amassian, *Adv. Funct. Mater.* **2016**, 26, 1737.
- [61] S. Mansouri, L. E. Mir, A. A. Al-Ghamdi, O. A. Al-Hartomy, S. A. F. A. Said, F. Yakuphanoglu, *Synth. Met.* **2013**, 185, 153.
- [62] S. Vegiraju, B.-C. Chang, P. Priyanka, D.-Y. Huang, K.-Y. Wu, L.-H. Li, W.-C. Chang, Y.-Y. Lai, S.-H. Hong, B.-C. Yu, C.-L. Wang, W.-J. Chang, C.-L. Liu, M.-C. Chen, A. Facchetti, *Adv. Mater.* **2017**, 29, 1702414.
- [63] S. Vegiraju, Y.-Y. Liu, K. Prabakaran, J.-S. Ni, Y. Ezhumalai, H.-C. Yu, S. L. Yau, J. T. Lin, M.-C. Chen, T.-C. Lin, *RSC Adv.* **2015**, 5, 54003.
- [64] L. S. Fuller, B. Iddon, K. A. Smith, *J. Chem. Soc., Perkin Trans.* **1997**, 1, 3465.
- [65] S. Vegiraju, G.-Y. He, C. Kim, P. Priyanka, Y.-J. Chiu, C.-W. Liu, C.-Y. Huang, J.-S. Ni, Y.-W. Wu, Z. Chen, G.-H. Lee, S.-H. Tung, C.-L. Liu, M.-C. Chen, A. Facchetti, *Adv. Funct. Mater.* **2017**, 27, 1606761.
- [66] J. Youn, S. Vegiraju, J. D. Emery, B. J. Leever, S. Kewalramani, S. J. Lou, S. Zhang, K. Prabakaran, Y. Ezhumalai, C. Kim, P.-Y. Huang, C. Stern, W.-C. Chang, M. J. Bedzyk, L. X. Chen, M.-C. Chen, A. Facchetti, T. J. Marks, *Adv. Electron. Mater.* **2015**, 1, 1500098.